Performance and radiation tolerance of InAs/GaSb LWIR detectors based on CBIRD design

Alexander Soibel, David Z.-Y. Ting, Sir. B. Rafol, Arezou Khoshakhlagh, Anita Fisher, Sam. A. Keo, and Sarath D. Gunapala

Infrared Photonics Group
Jet Propulsion Laboratory
California Institute of Technology

Outline

- Introduction
  - Barrier Infrared Detector (BIRD)
  - Complementary Barrier Infrared Detector (CBIRD)
- CBIRD focal plane array (FPA)
- Single pixel device performance vs FPA
- Proton radiation effect on CBIRD performance
  - Dark current
  - Spectral characteristics
- Summary

Antimonides Material System for Type-II Superlattices

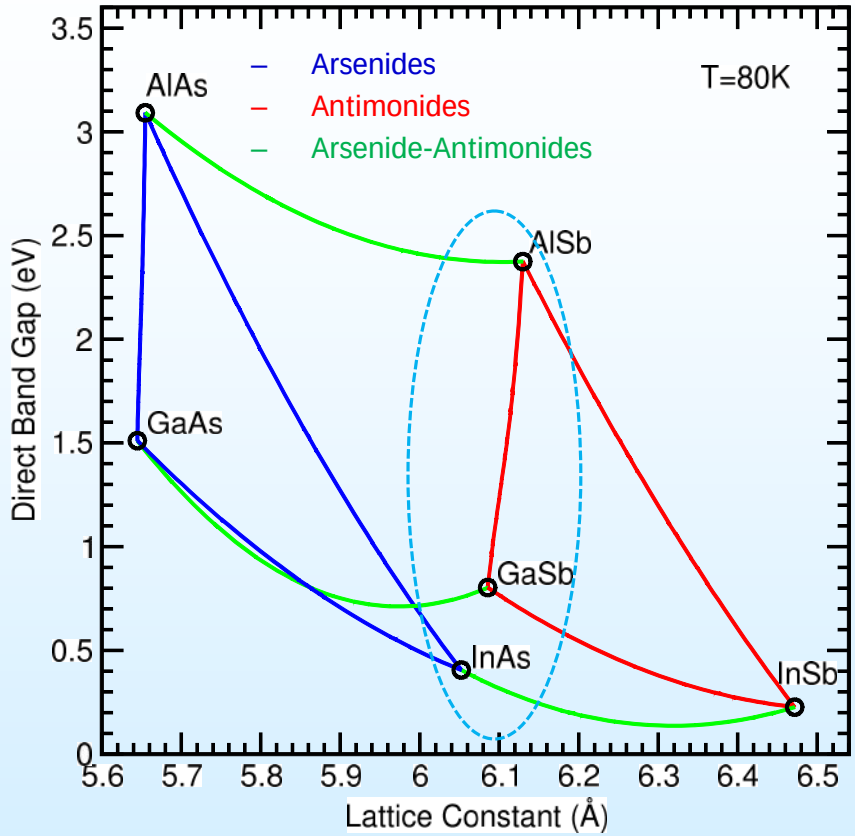

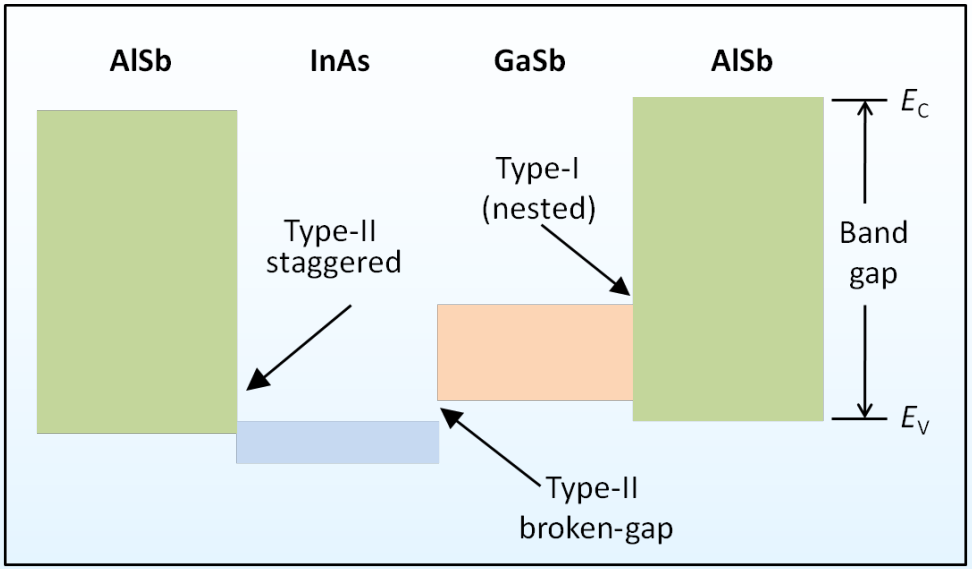

- Material system includes InAs, GaSb, AlSb and their alloys
  - Nearly lattice matched (~6.1 Å)
- Alloys with GaAs, AlAs, and InSb adds even more flexibility

- Three types of band alignments
  - Type-I (nested, straddling)
  - Type-II staggered
  - Type-II broken gap (misaligned, Type-III)
    - Unique among common semiconductor families
    - Overlap between InAs CB and GaSb VB enables interband devices
- Tremendous flexibility in artificially designed materials / device structures

Copyright 2012. All rights reserved.

Key Properties of Type-II Superlattices

- Infrared band gap
  - SWIR to VLWIR
- Absorption strength comparable to MCT

Advantages:

- Lower tunneling leakage
- Reduced diffusion dark current (p-type)
- Reduced Auger generation

Challenges:

- G-R dark current induced by SRH processes
- Lifetime significantly lower than MCT
  - Attributed to SRH
  - Effect of short lifetime on diffusion dark current ?
- Surface leakage

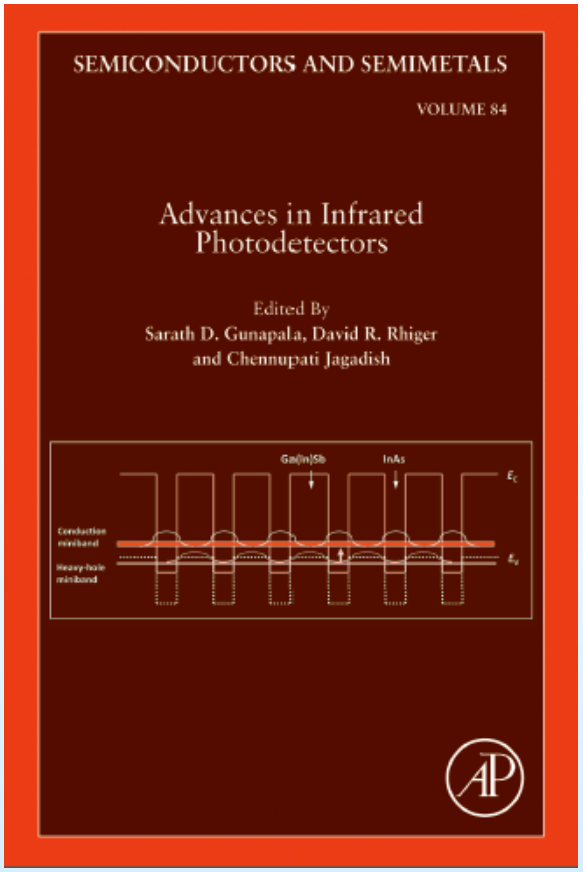

"Type-II Superlattice Infrared Detectors", *D. Z. Ting, A. Soibel, L. Höglund, J. Nguyen, C. J. Hill, A. Khoshakhlagh, and S. D. Gunapala, Semiconductors and Semimetals* **84**, pp.1-57 (2011).

G-R Dark Current Suppression using Unipolar Barriers

Barrier Infared Detector (BIRD)

- Homojunction LWIR superlattice detectors have limited performance
  - p-n, p-i-n diodes
  - Good responsivity and QE
  - High dark current

- Designs based on heterostructures can enhance performance
  - Barriers can reduce dark current
  - But do not want to cut down responsivity/QE
  - "Unipolar barriers" are particularly useful in this respect

Unipolar Barriers

Electron blocking barrier

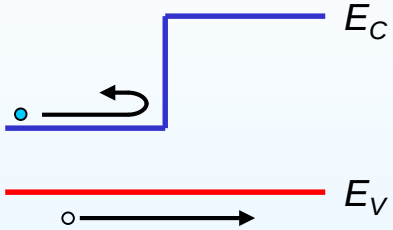

Hole blocking barrier

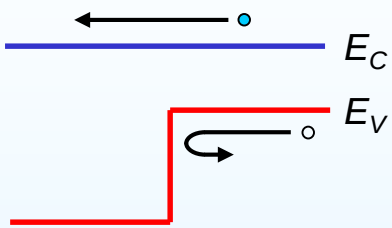

- Unipolar barriers:
  - Block one carrier type, but allows un-impeded flow of the other
  - Electron barrier
  - Hole barrier
  - Terminology introduced in Ting et al. *Appl. Phys. Lett.* **95**, 023508 (2009), now in common usage

Double Heterostructure Laser

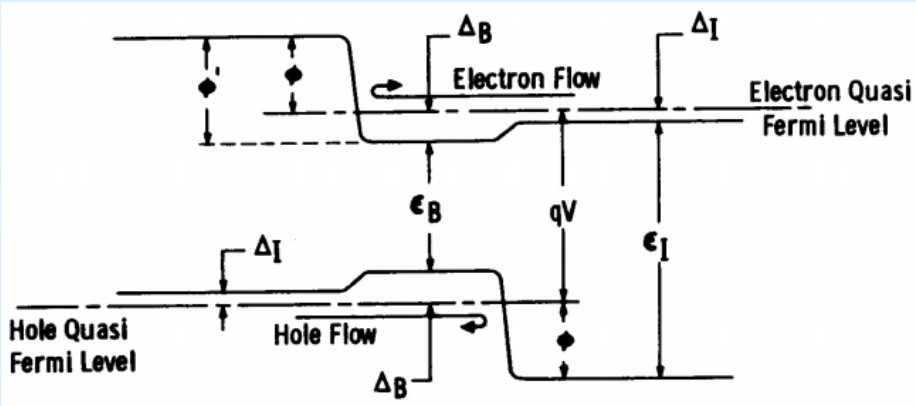

- Using unipolar barriers to enhance semiconductor device performance
  - DH Laser, H. Kroemer, Proc. IEEE 1963
  - DH Laser, Zh. I. Alferov and R. F. Kazarinov, patent certificate (Russian) 1963

Copyright 2011. All rights reserved.

SRH Suppression in LWIR SL Heterodiode

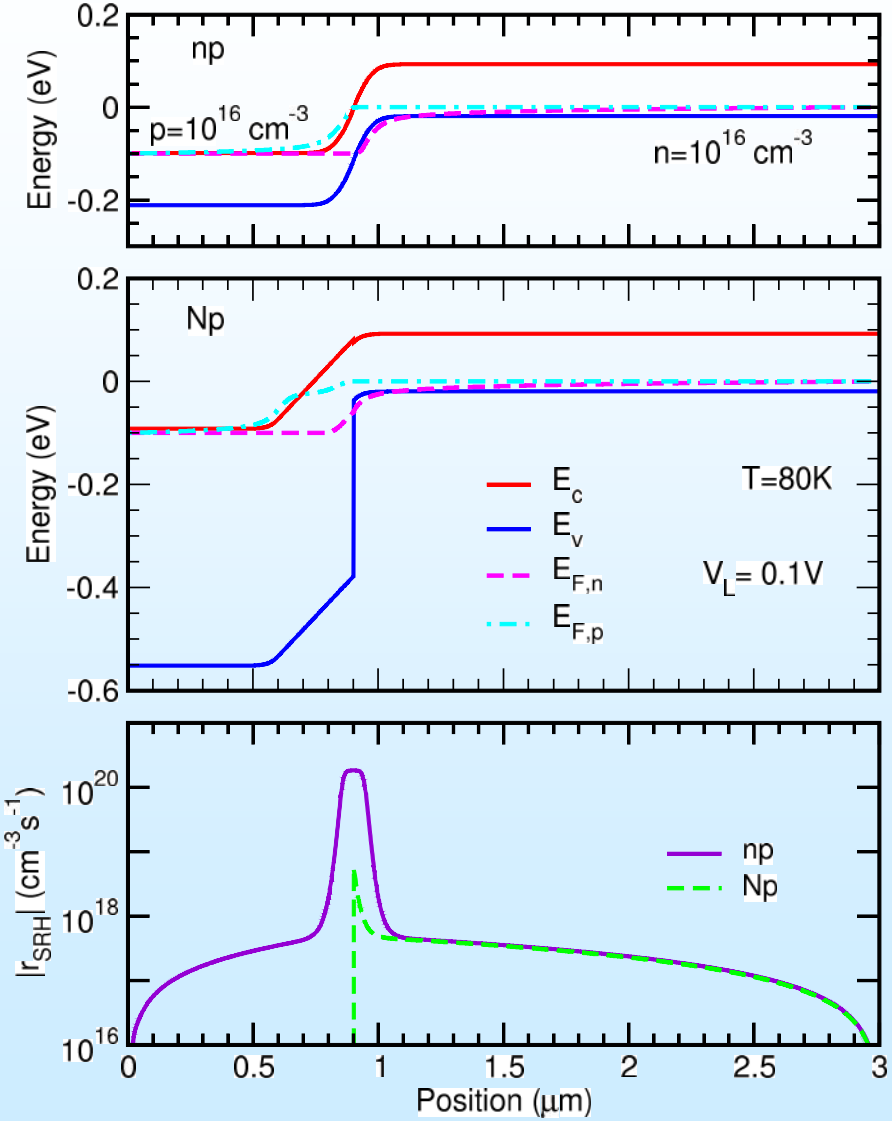

- Drift-diffusion simulation comparing LWIR SL np and Np diodes
- np homodiode
  - LWIR InAs/GaSb SL
- Np heterodiode
  - LWIR InAs/AlSb SL p-type absorber
  - InAs/AlSb SL hole-blocking unipolar barrier
  - Hole barrier does not block photocurrent
- SRH recombination rate given by

$$r_{SRH} = (np - n_i^2) / [(\tau_p (n + n_i) + (\tau_n (p + p_i)]$$

- The Np heterostructure can be effective at SRH suppression

CBIRD Structure

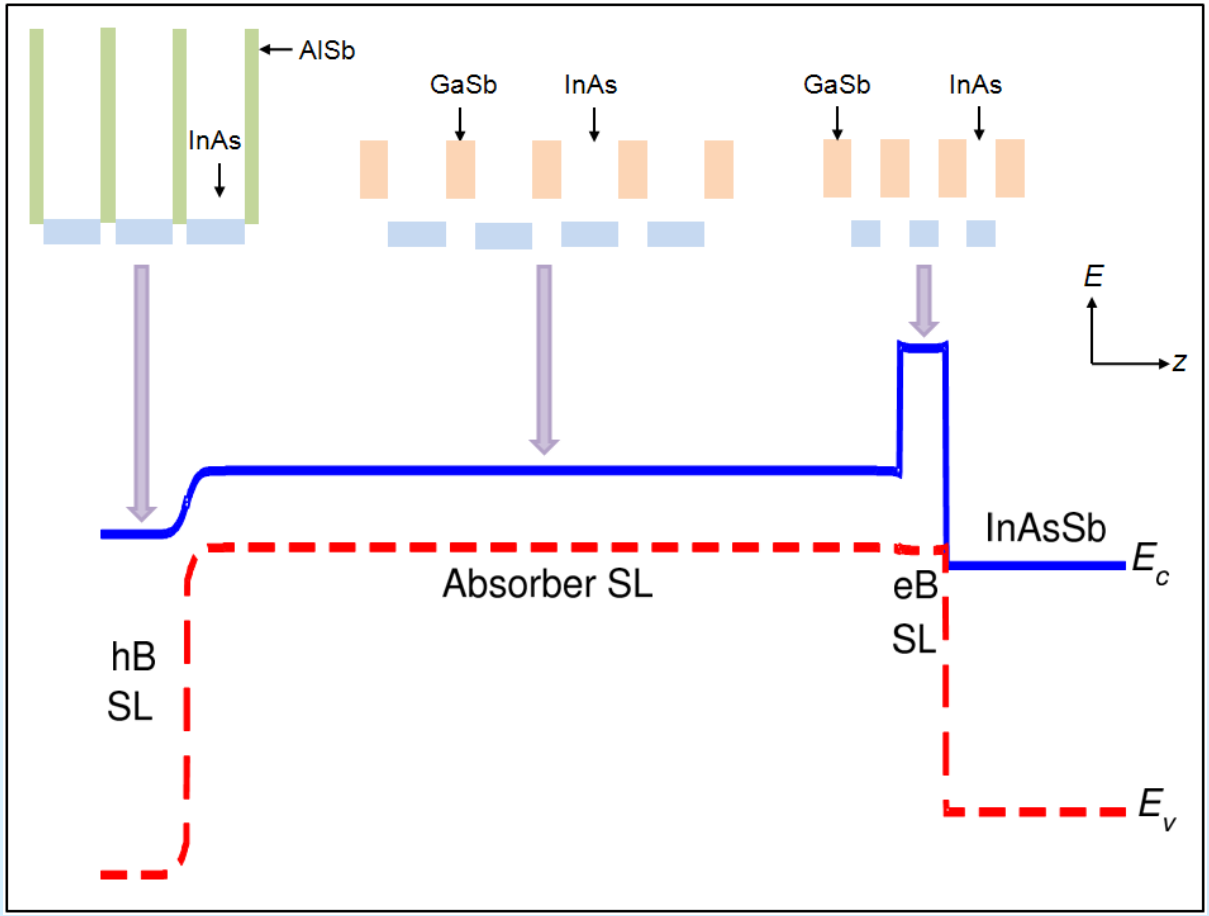

- Complementary Barrier Infrared Detector (CBIRD)
- p-type LWIR superlattice absorber surrounded by
  - n-doped unipolar hole barrier (hB)
  - p-doped unipolar electron barrier (eB)
- Bottom tunneling contact

Copyright 2011. All rights reserved.

CBIRD Characteristics

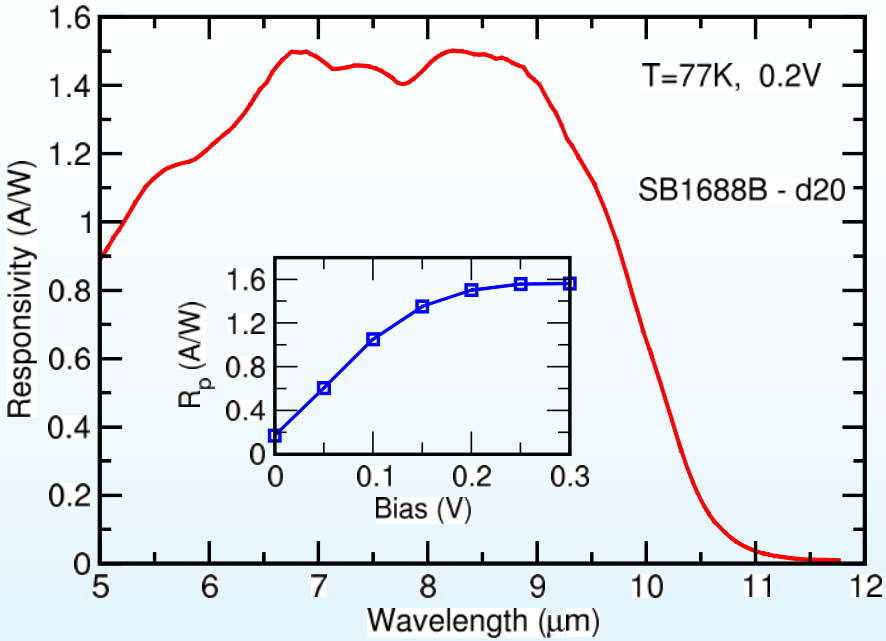

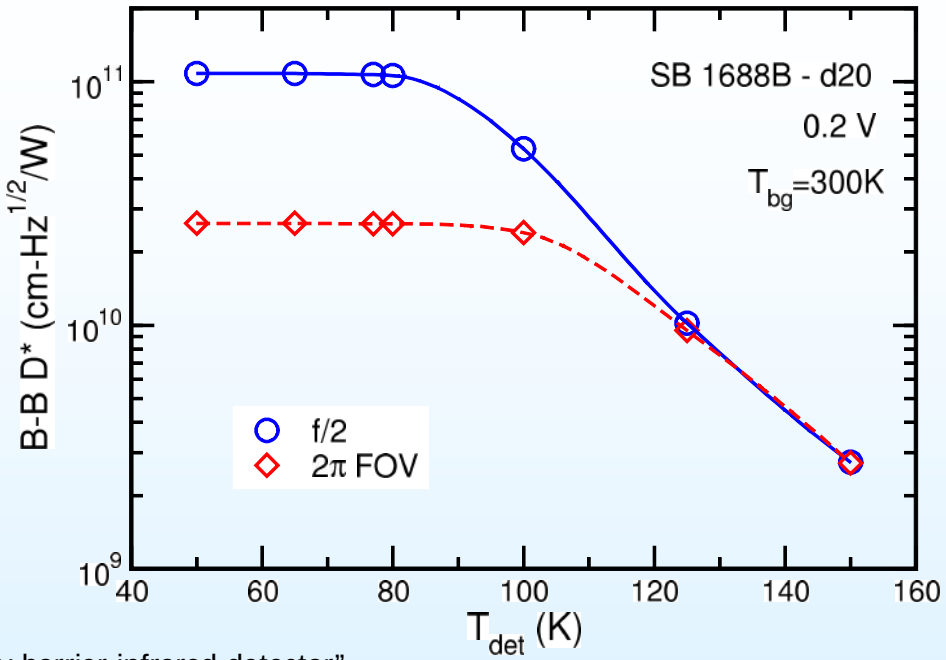

"A high-performance long wavelength superlattice complementary barrier infrared detector",
D. Z.-Y. Ting, C. J. Hill, A. Soibel, S. A. Keo, J. M. Mumolo, J. Nguyen, S. D. Gunapala, *Appl. Phys. Lett.* **95**, 023508 (2009).

- Discrete 220 μm × 220 μm devices
- 10 μm cutoff (50% peak responsivity)
- R_{peak} = 1.5 A/W at 0.2 V (λ_p=8.2 μm);
  - QE=27% (single pass, no AR coating)
- J_d(0.2V, 77K) = 1x10^{-5} A/cm^2
- Black-body D* (8 μm to 10 μm; 300K background), f/2 optics:
  - T_{BLIP}= 86K, (BLIP condition: I_{dark} < ¼ I_{photo})
  - B-B BLIP *D** = 1.1×10^{11} cm-Hz$^{1/2}$/W

Copyright 2011. All rights reserved.

Noise Measurement: Frequency and Bias Dependence

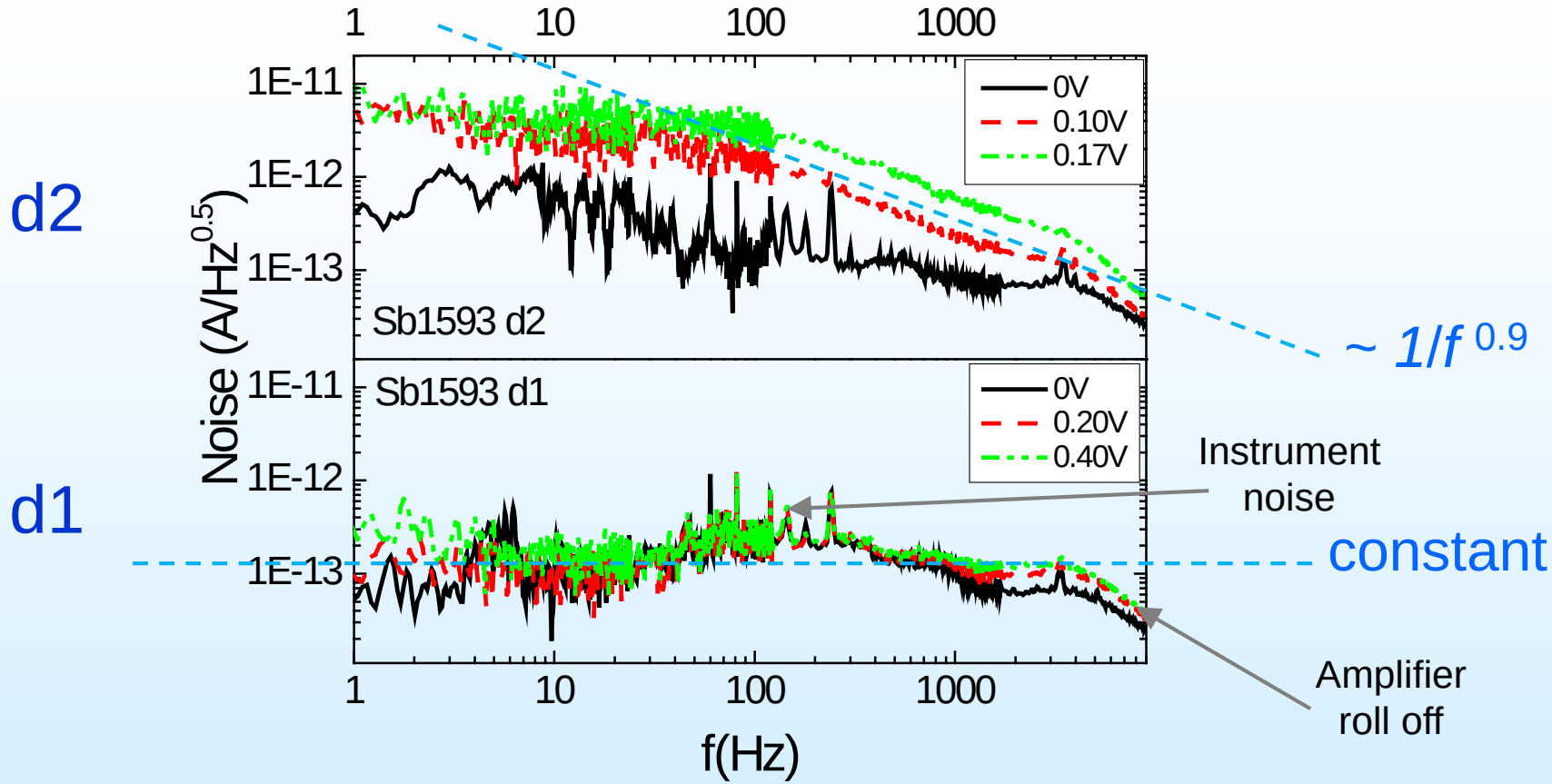

- Superlattice photodetectors studied exhibit no intrinsic (bulk) high 1/f noise
- Measurements clearly show that sidewall leakage current contributes to:
  - increased shot noise (from higher dark current)
  - also additional frequency dependent noise

Appl. Phy. Lett. **96**(11), 111102 (2010).

Optical studies of InAs/GaSb superlattices

$$\frac{1}{\tau} =$$

We performed optical studies of InAs/GaSb superlattices:

- Absorption,
- Phot luminescence
- Minority carrier lifetime
- Lifetime temperature dependence

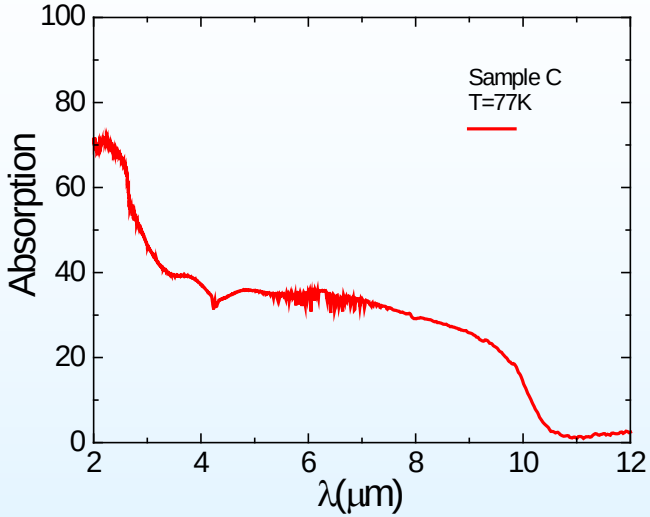

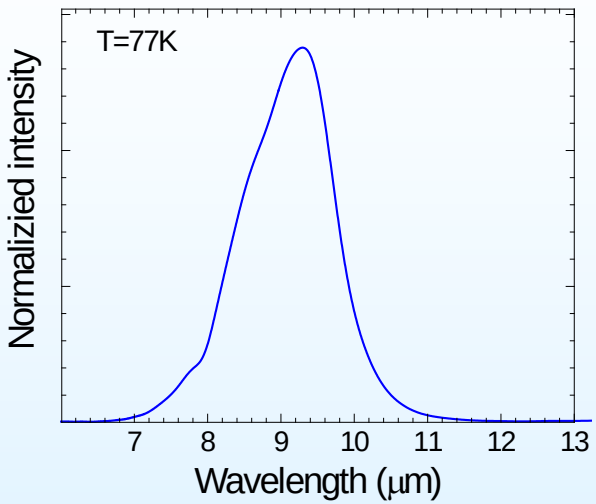

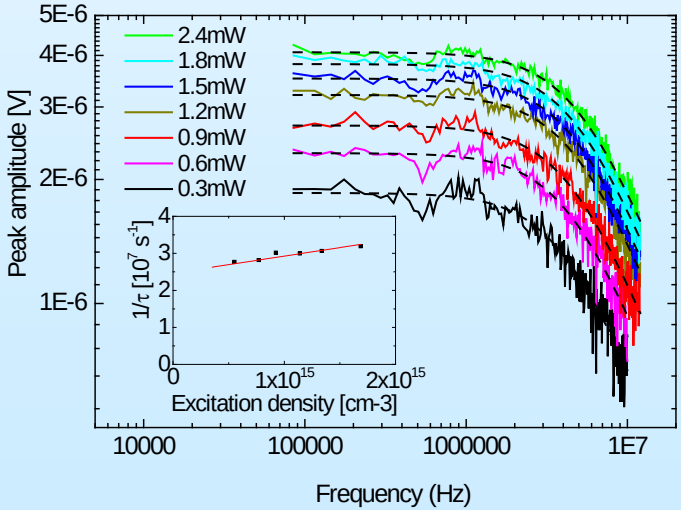

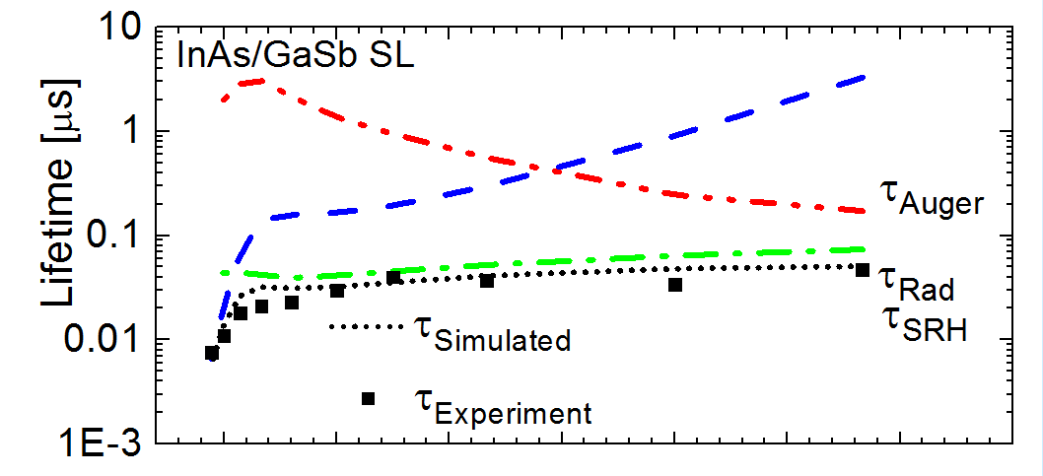

Hoglund et al. Appl. Phys. Lett. 103, 221908 (2013)

Outline

- Introduction
  - Barrier Infrared Detector (BIRD)
  - Complementary Barrier Infrared Detector (CBIRD)
- **CBIRD focal plane array (FPA)**
- Single pixel device performance vs FPA
- Proton radiation effect on CBIRD performance
  - Dark current
  - Spectral characteristics
- Summary

Material Growth and Characterization

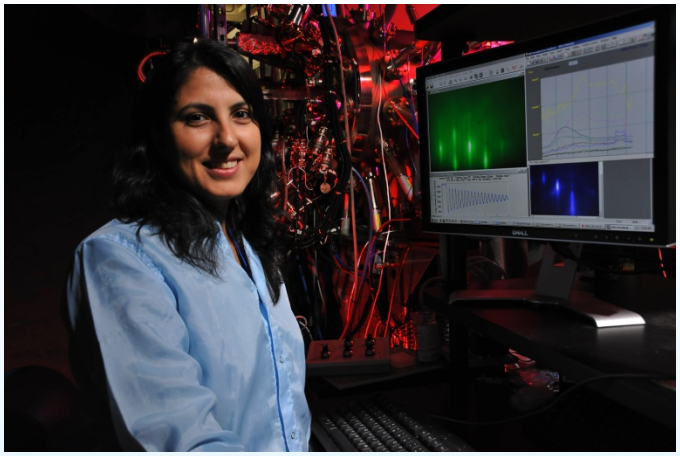

Gen-III MBE:
Superlattice growth

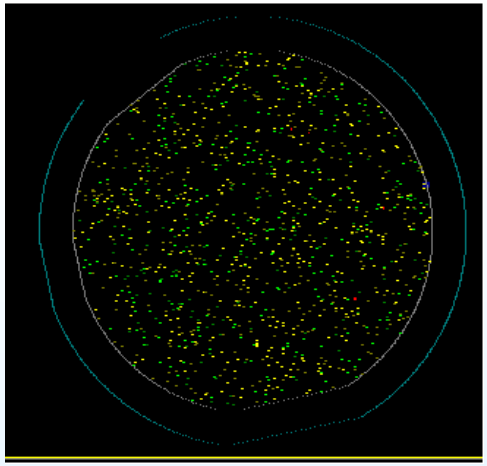

Surfscan: surface-quality

Particle count: 77.4/cm^2

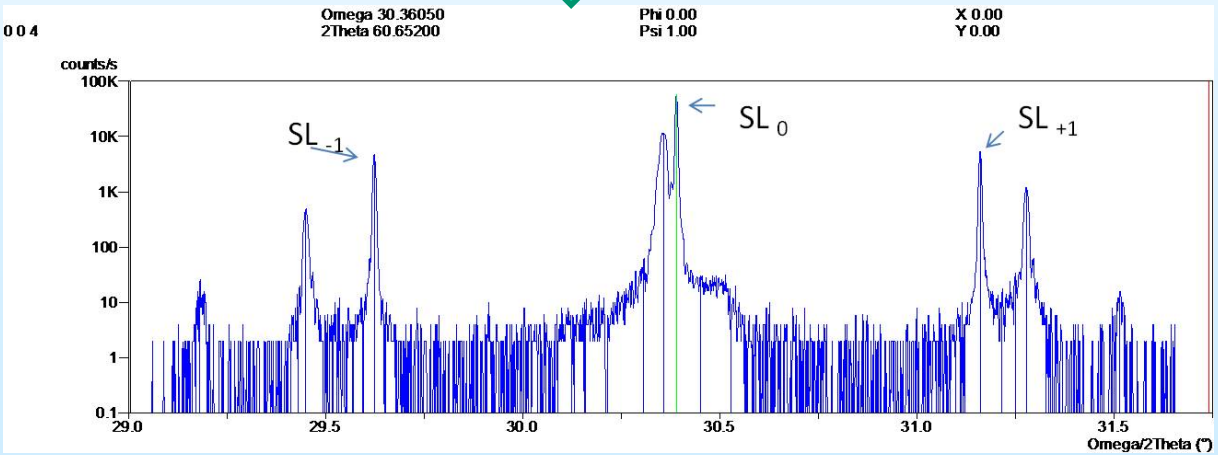

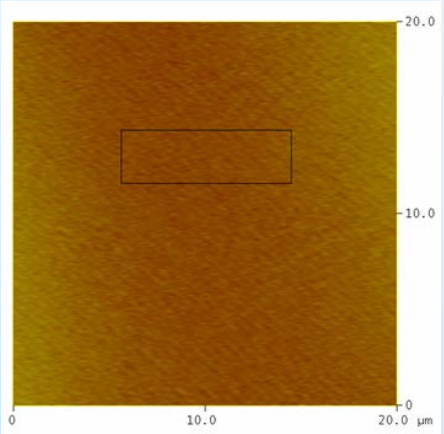

AFM: Surface morphology
20 µm x 20 µm scan
Defect free surface

XRD: Structural quality
Period: 66.4 Å
Average FWHM $SL_{+1,-1}$=21.67 arcsec

Copyright 2011. All

Combination Dry Etch

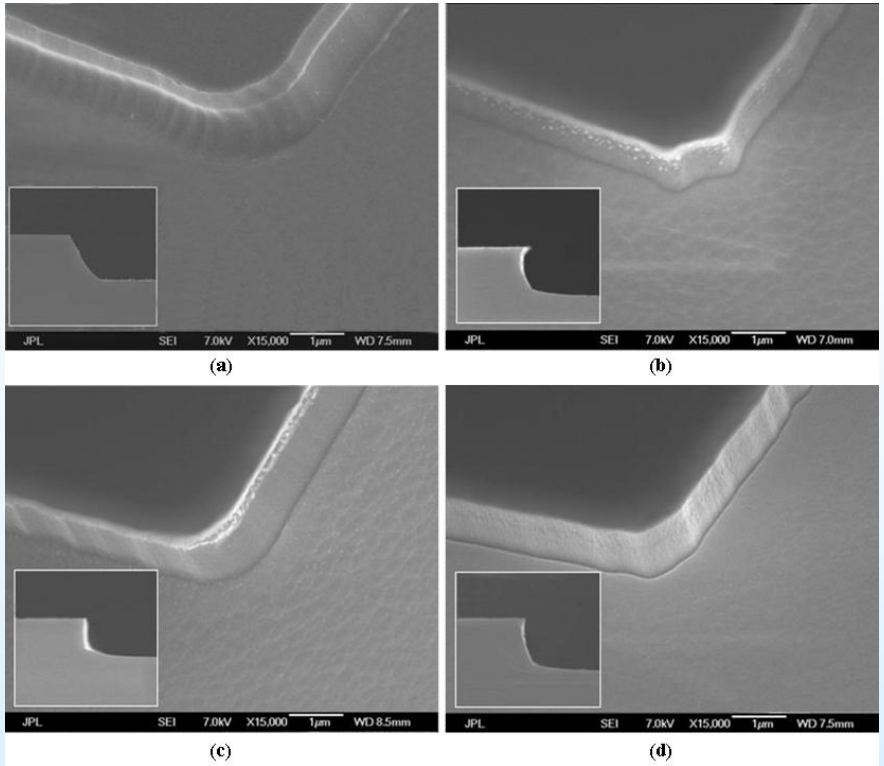

"Low dark current long-wave infrared InAs/GaSb superlattice detectors",

Jean Nguyen, A. Soibel, D. Z.-Y. Ting, C. J. Hill, M. C. Lee, and S. D. Gunapala,

Appl. Phy. Lett. **97**(5), 051108 (2010).

- $CH_4/H_2/BCl_3/Cl_2/Ar$ combination ICP dry etch technique
- Variable device size study shows lowest surface-to-bulk dark current ratio among several etch techniques
- Combination etch produced nearly vertical, smooth side walls
  - High fill factor favorable for FPA fabrication
  - Minimal dielectric mask erosion

Copyright 2012. All rights reserved.

CBIRD FPA

- ISC-0903 ROIC, 320x256 format, fully delineated
- T= 78K operating temperature, 300K background, f/2 optics
- Operability ~ 97% [$0.75*R_{MEAN} < R < 1.25*R_{MEAN}$]
- QE ~ 45% (4.5 – 9 µm)
- NEDT ~ 18.6 mK

CBIRD FPA

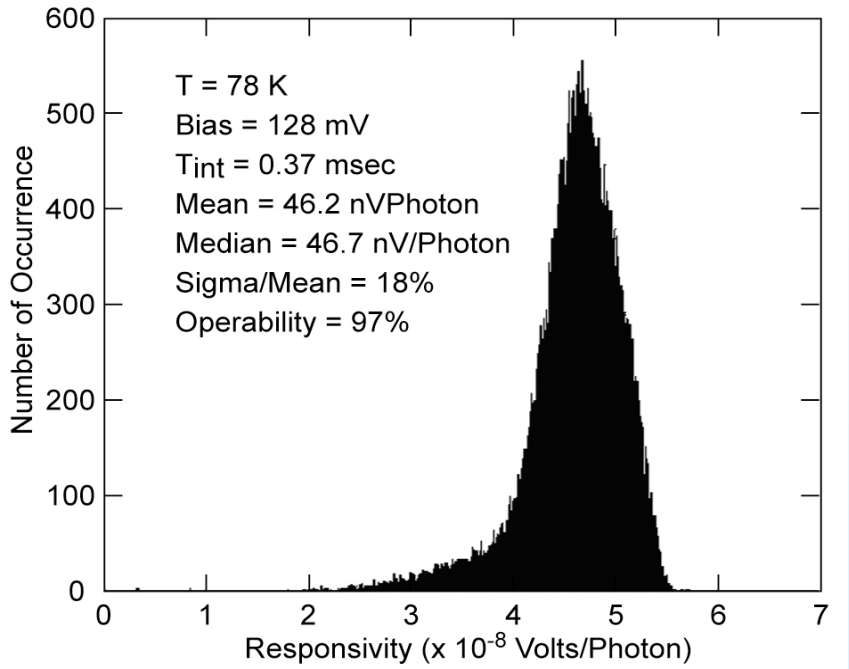

Responsivity histogram at 78 K operating temperature for an n-CBIRD FPA

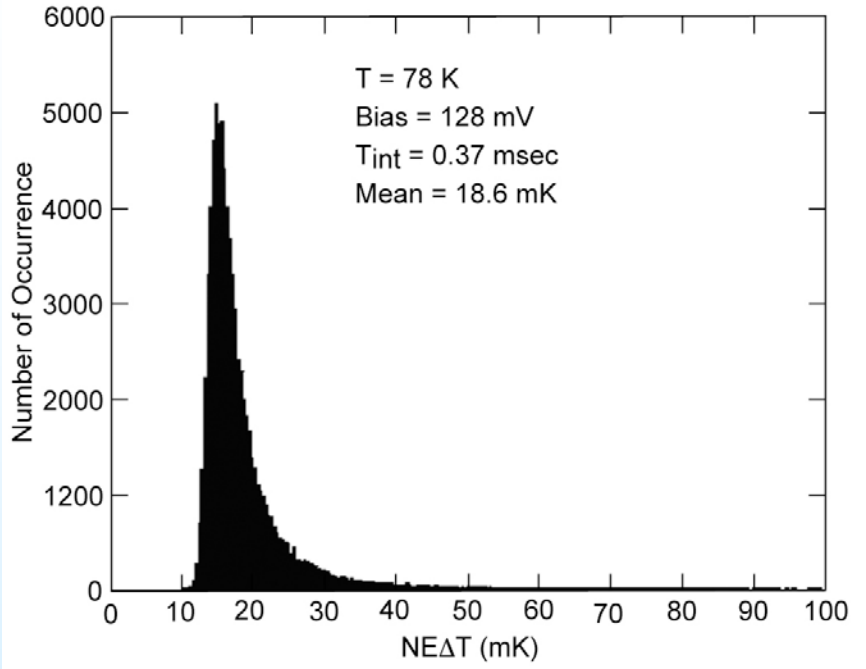

Measured n-CBIRD NEDT histogram operating at 78 K, bias of 128 mV and integration time of 370 msec. The mean NEDT is 18.6 mK

- Operability ~ 97% $[0.75*R_{MEAN} < R < 1.25*R_{MEAN}]$
- NEDT ~ 18.6 mK
- This value of NEDT implies good noise properties of detector and ROIC

Outline

- Introduction
  - Barrier Infrared Detector (BIRD)
  - Complementary Barrier Infrared Detector (CBIRD)
- CBIRD focal plane array (FPA)
- **Single pixel device performance vs FPA**
- Proton radiation effect on CBIRD performance
  - Dark current
  - Spectral characteristics
- Summary

Spectral Response

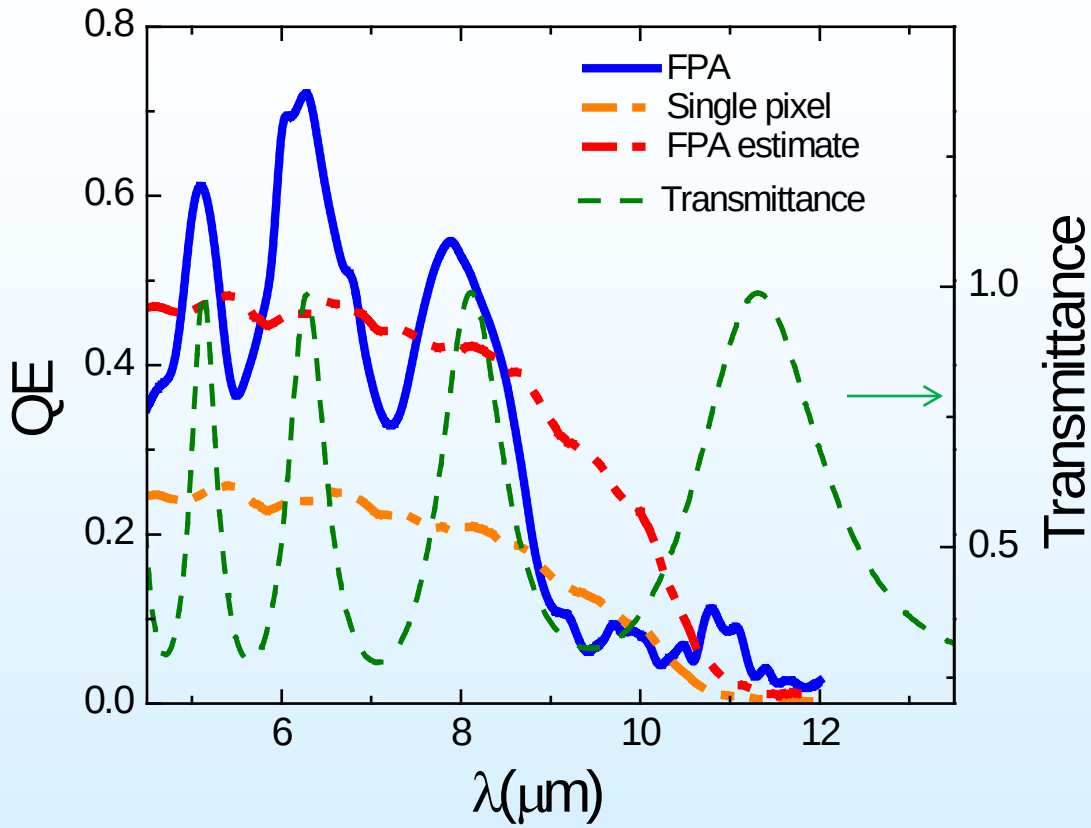

We attributed oscillations observed in FPA spectral curve to the Fabry-Perot oscillations resulting from full reflection at the top metal contact and partial reflection at backside/air interface that has reflectivity of about 30%.

FPA: QE of 50 % is for back illuminated FPA with substrate completely removed and without antireflection (AR) coating. The cuf-off wavelength defined at 50% of the peak is about λ = 8.8μm

PEC: QE of about 25% is for single pass, and QE estimate for multipass absorption characteristic for FPAs is 45%. The PEC cut-off is 9.9μm; and PEC spectrum does not exhibit any oscillations.

Copyright 2012. All rights reserved.

CBIRD with Zero Turn-On Bias

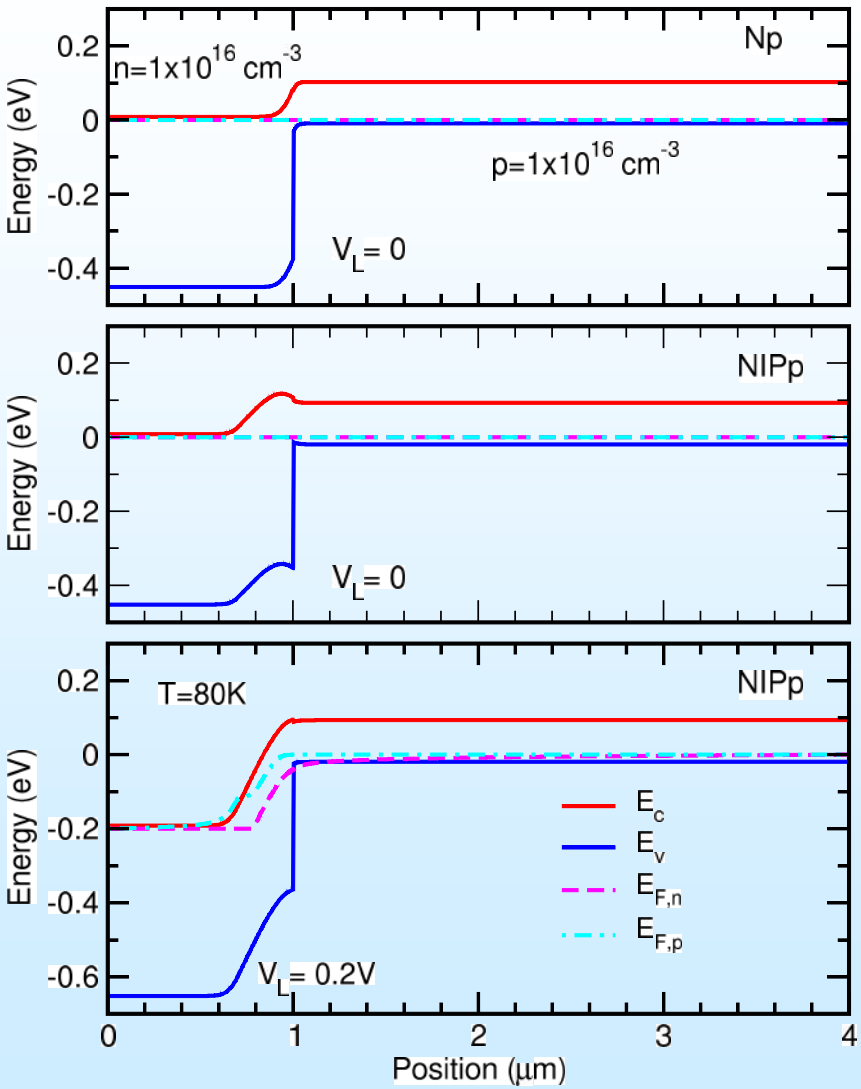

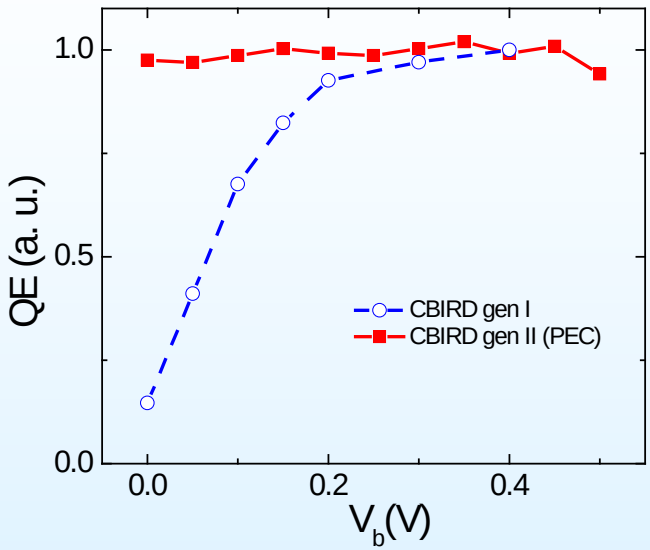

- The 200 mV turn-on bias in original CBIRD device attributed to un-intended electron barrier at the hole-barrier/ absorber interface
- Attributed to unintended conduction band offset or dopant migration (see figure at left)
- New CBIRDs turn on at zero bias

Copyright 2012. All rights reserved.

Dark current: Single pixel

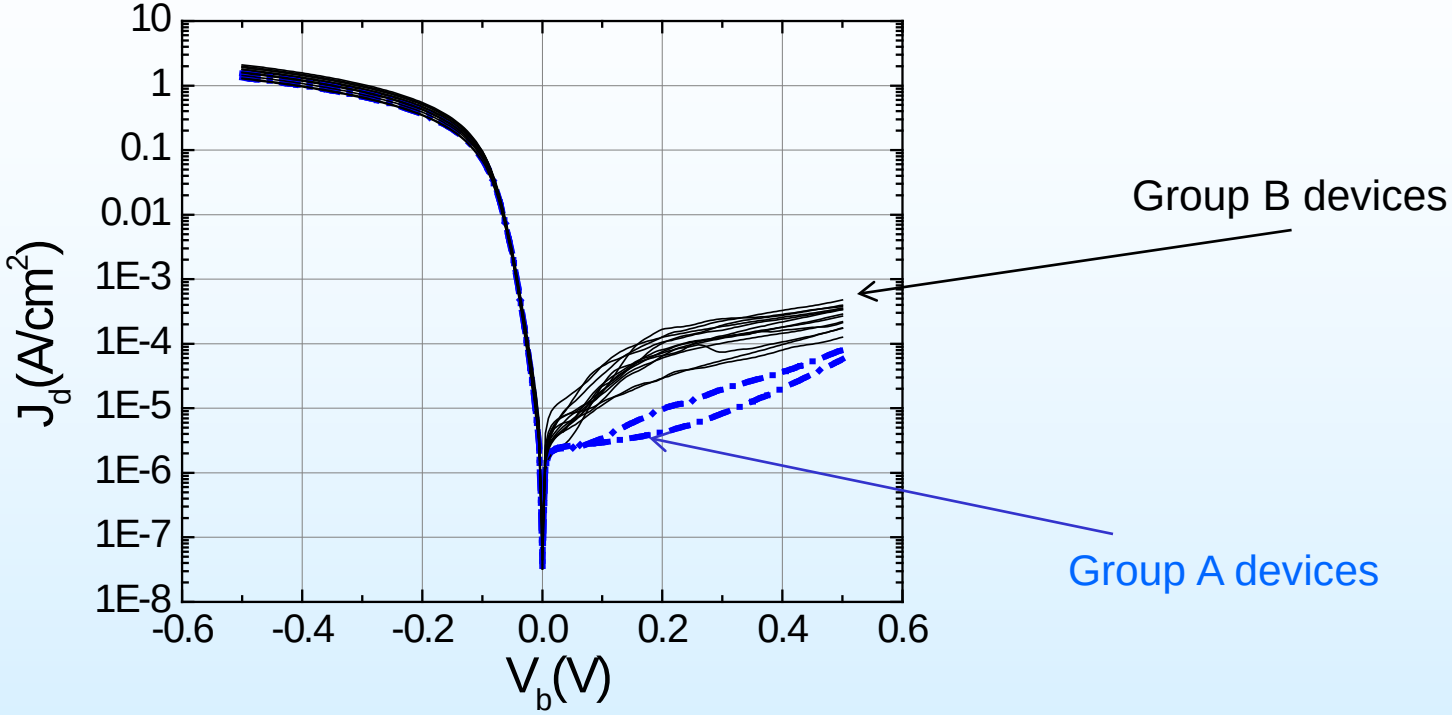

Dark current density of fifteen 200μm square PEC photodiodes operating at T = 77K

- Most of the devices have dark current density $j_d = 2\text{x}10^{-5}$ A/cm^2 at $V_b = 0.1$V
- Two photodiodes exhibit much lower dark current density $j_d = 3*10^{-6}$ A/cm^2

Copyright 2012. All rights reserved.

Dark current vs. temperature

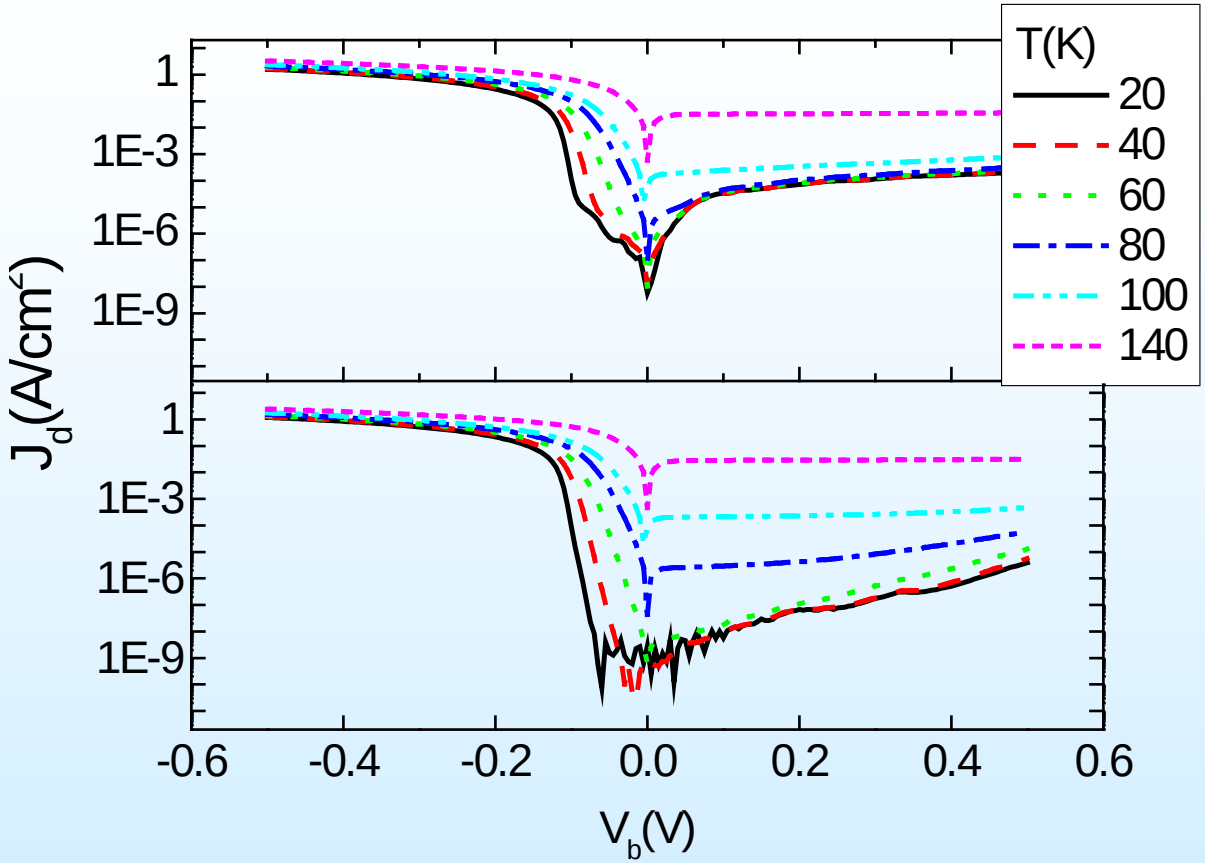

The dark current density in devices A (bottom) and B (top) as a function of applied bias, measured at various temperatures ranging from 20 to 140 K

Copyright 2012. All rights reserved.

Dark current vs. temperature

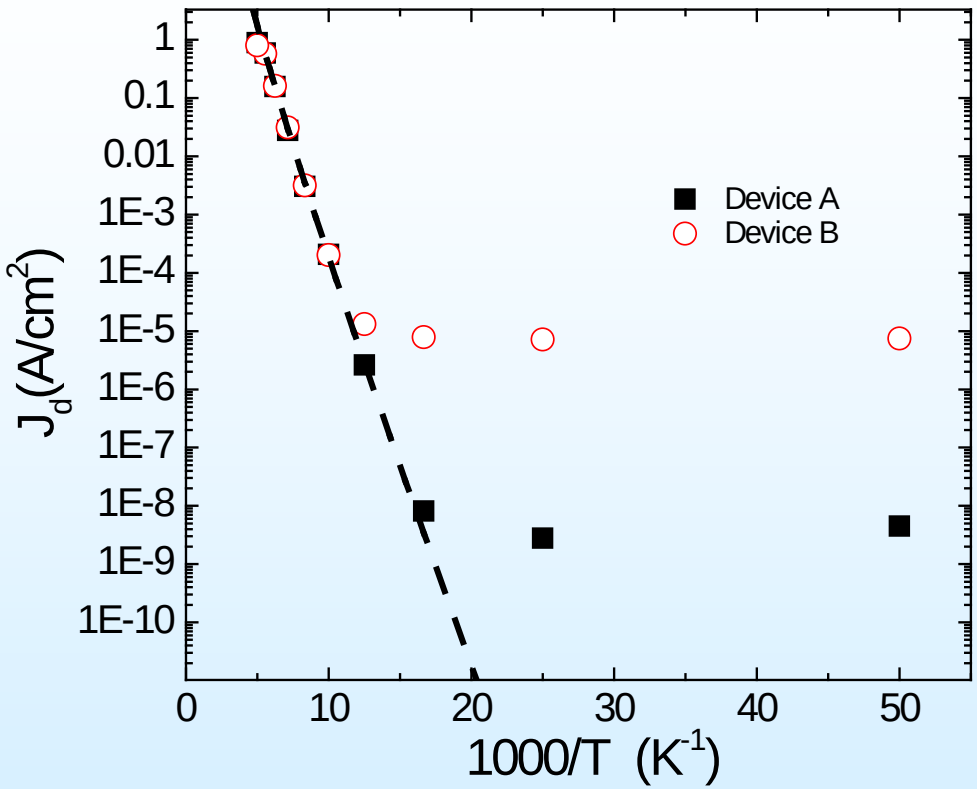

The dark current density versus inverse photodiode temperature, measured at applied bias Vb = 0.1 V.

Dark current fit (the dashed line): $j_d \sim T^3 \exp(-Eg/k_B T)$,

with $E^f g$ = 9.9μm found from the fit to the data is equal to the superlattice bandgap Eg = 9.9μm

j_d is diffusion limited at low bias in both sets of devices at above 100K

- At temperatures above 100K the current densities of both devices are very close to each other
- The dark current in the device "A" continue to decrease with the temperature down to about *T* = 60K, when in the device "B" dark current become temperature independent around 90K

Copyright 2012. All rights reserved.

CBIRDs with Zero Turn-On Bias

The exact dark current mechanisms in these two groups of devices represented by diodes "A" and "B" are still under investigation so we can only speculate about origin of the observed difference at this point.

Intrinsic material or CBIRD design properties such as Auger recombination or band-to-band tunneling:
- All devices would be affected by that

The side wall surface leakage current associated with the properties of dangling bonds on the exposed side wall:
- All devices would be affected by that; contradicts to our study of the dark current in the variable area devices

Material disorder
- Most common: generation-recombination current arising from SRH recombination: have $j_d \sim \exp(-Eg/2kBT)$ dependence rather than the observed temperature independent dark current
- Large microscopic defects: The material quality is very high as was assessed by AFM and surfscan, and the dark current density is still low ($j_d < 10^{-4}$ A/cm^2 at $V_b = 0.1$V) even in the group B devices
- Dislocations that were demonstrated to be source of relatively low extraneous dark current in these devices (Serguei I. Maximenko and Ed. Aifer, NRL; private communication)

Surface disorder located close to electron or hole barriers that can serve as surface leakage shunts
- These particular wafers are more sensitive than our previous devices to defect mediated side wall surface leakage current due to absence of extra barrier in the conduction band

Copyright 2012. All rights reserved.

Dark current: Single pixel vs FPA

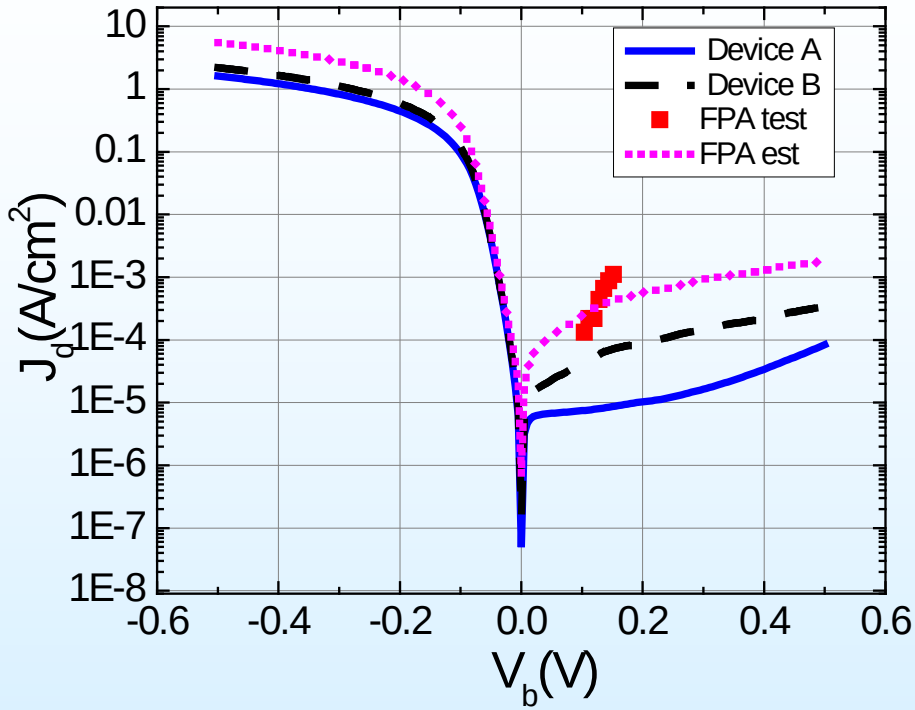

The dark current density in the FPA is by order magnitude higher than in the group B devices and by two orders of magnitude than in groups A devices.

<u>FPA dark current estimate</u>

-Assume j_d at T = 77K in the group A devices is good estimation for the bulk current density.

-The surface leakage current is estimated from the difference of j_d between group A and B devices,

- Assuming linear dependence of surface defects number on pixel size

The estimated dark current density in FPA offers good agreement with measured FPA j_d around operational bias V_b=0.1V.

Copyright 2012. All rights reserved.

Outline

- Introduction
  - Barrier Infrared Detector (BIRD)
  - Complementary Barrier Infrared Detector (CBIRD)
- CBIRD focal plane array (FPA)
- Single pixel device performance vs FPA
- **Proton radiation effect on CBIRD performance**
  - Dark current
  - Spectral characteristics
- Summary

Detector performance

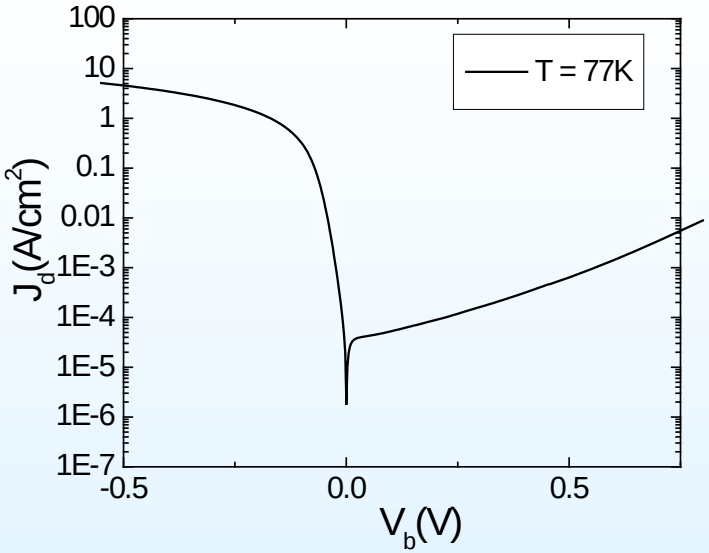

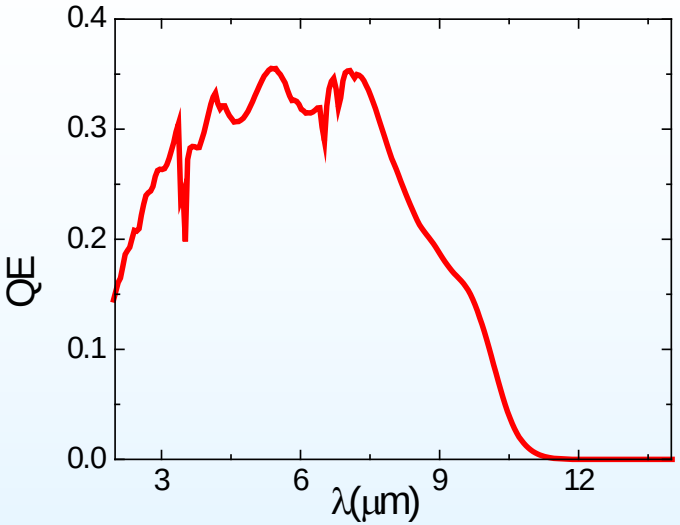

Dark current $j_d = 5\text{x}10^{-5}$ A/cm^2 at $V_b = 0.1$V

Cut-off wavelength, $\lambda_c = 10.2\mu$m, was found from the inflection point

The maximal QE, $QE_{max} \approx 0.35$ was measured at $\lambda = 7\mu$m

- narrow bandpass filter centered at $\lambda_B = 8.6\mu$m to measure the detector photoresponse during the irradiation studies
- $QE_B \approx 0.24$ measured at $\lambda_B = 8.6\mu$m

Zero turn-on bias

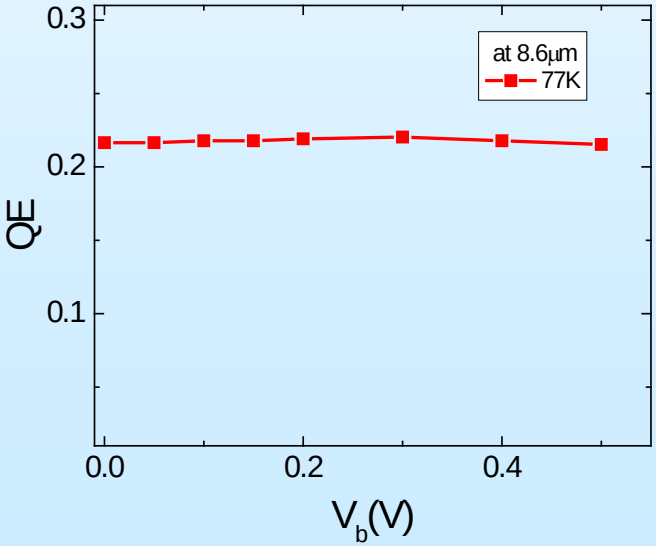

Copyright 2011. All rights reserved.

Radiation details / test

The 68MeV proton exposure was performed at cyclotron at UCD

Each radiation session was about 15 min

Detectors were kept at T = 80K for duration of the study

Detectors were kept unbiased during irradiation

Dark current and photoresponse were tested prior to the irradiation and after each dose

1. Ionization damage
   - Creates *e-h* pairs

     Charge can be trapped at semiconductor-insulator interface
   - Units: 1 rad = 0.01 J/kg

2. Displacement damage
   - Results in lattice defects
   - Units: Displacement Damage Dose (DDD) [MeV/g]

     DDD = $S \times \Phi p$,

     Φp is particle fluence

     $S = 3.3\times10^{-3}$ MeVcm^2/g for GaSb and 68 MeV protons

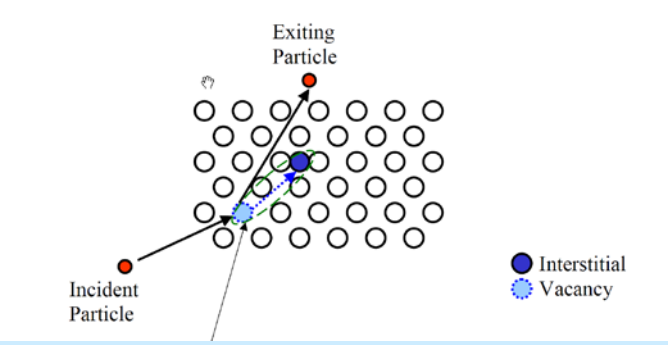

Displacement damage

Fluency [10^{11} H^+/cm^2]	Total Ionizing Dose (TID) [kRad]	Displacement damage dose (DDD) [10^9 MeV/g]
0	0	0
1.4	15	0.48
2.8	30	0.95
4.8	50	1.6
7.2	75	2.4
9.6	100	3.2
14.4	150	4.8
19.2	200	6.4

Copyright 2011. All rights reserved.

Dark current density at T = 80K

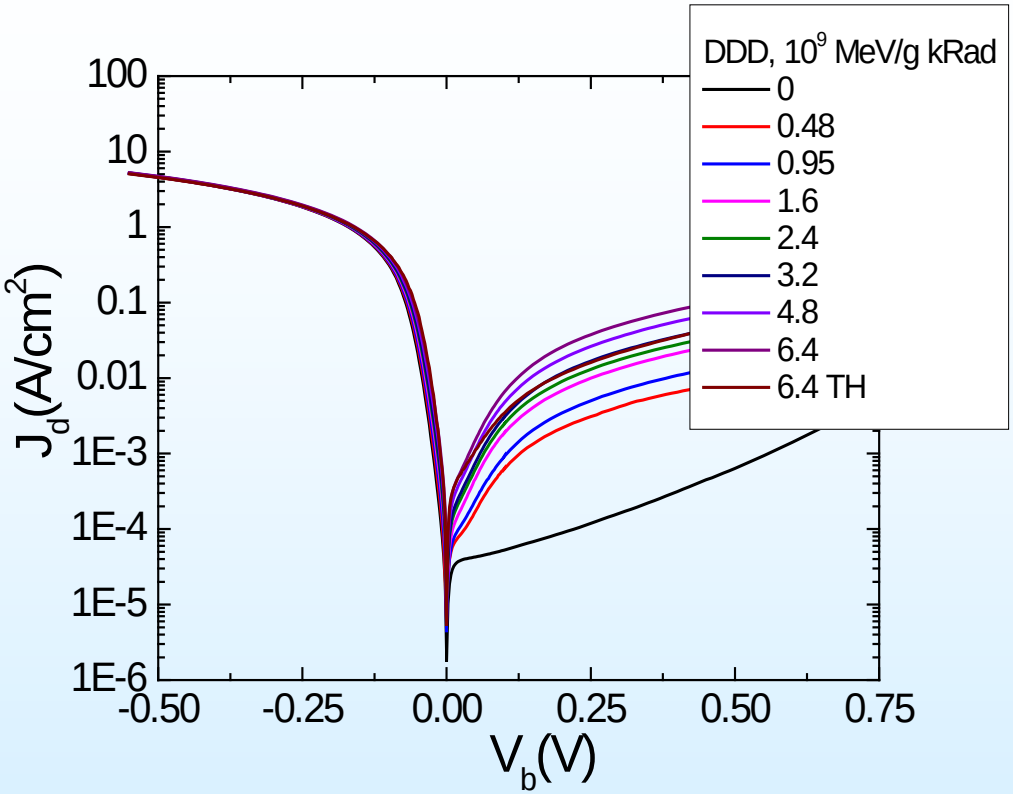

DDD [10^9 MeV/g]	TID [kRad]	J_d [A/cm^2]
0	0	5×10^{-5}
0.48	15	6×10^{-4}
6.4	200	6×10^{-3}

- Shape of *j(V)* curves exhibits a pronounced change following the first irradiation.
- Dark current density of these devices increases with DDD
- Detector thermocycling ((keeping the detector at room temperature for three months) resulted only in a small reduction of dark current to $j_d = 4 \times 10^{-3}$ A/cm^2
  - The radiation damage is not annealed at room temperature
  - Can be attributed to the displacement effects

Copyright 2011. All rights reserved.

Dark current density vs dose

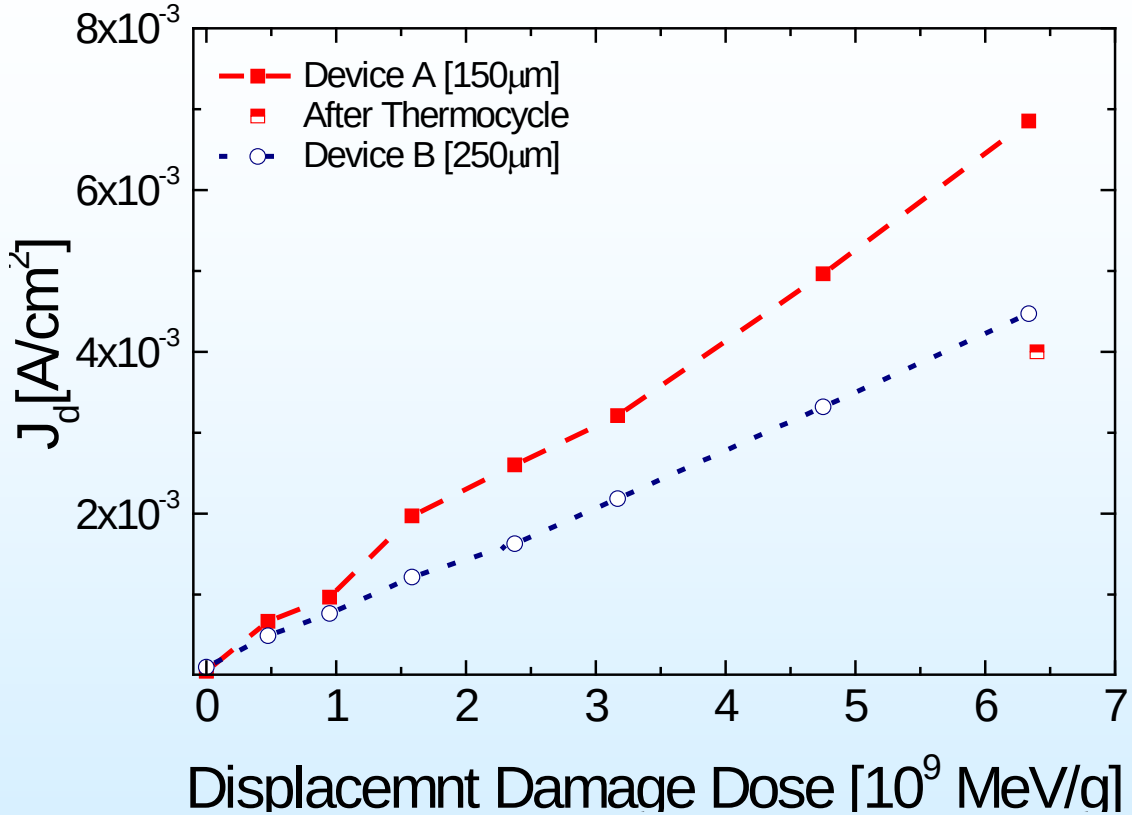

- Dark current increase linearly with DDD, as $j_d = j_{d0} + K_{jd}\Phi p$, where
  - K_{jd} is the dark damage factor
  - Φp is the proton irradiation fluence.
- Fit to data gives $K_{jd} \approx 2.2 - 3.5\times10^{-15}$ (A/cm^2) /(H$^+$/cm^2).

Copyright 2011. All rights reserved.

Dark current at different T

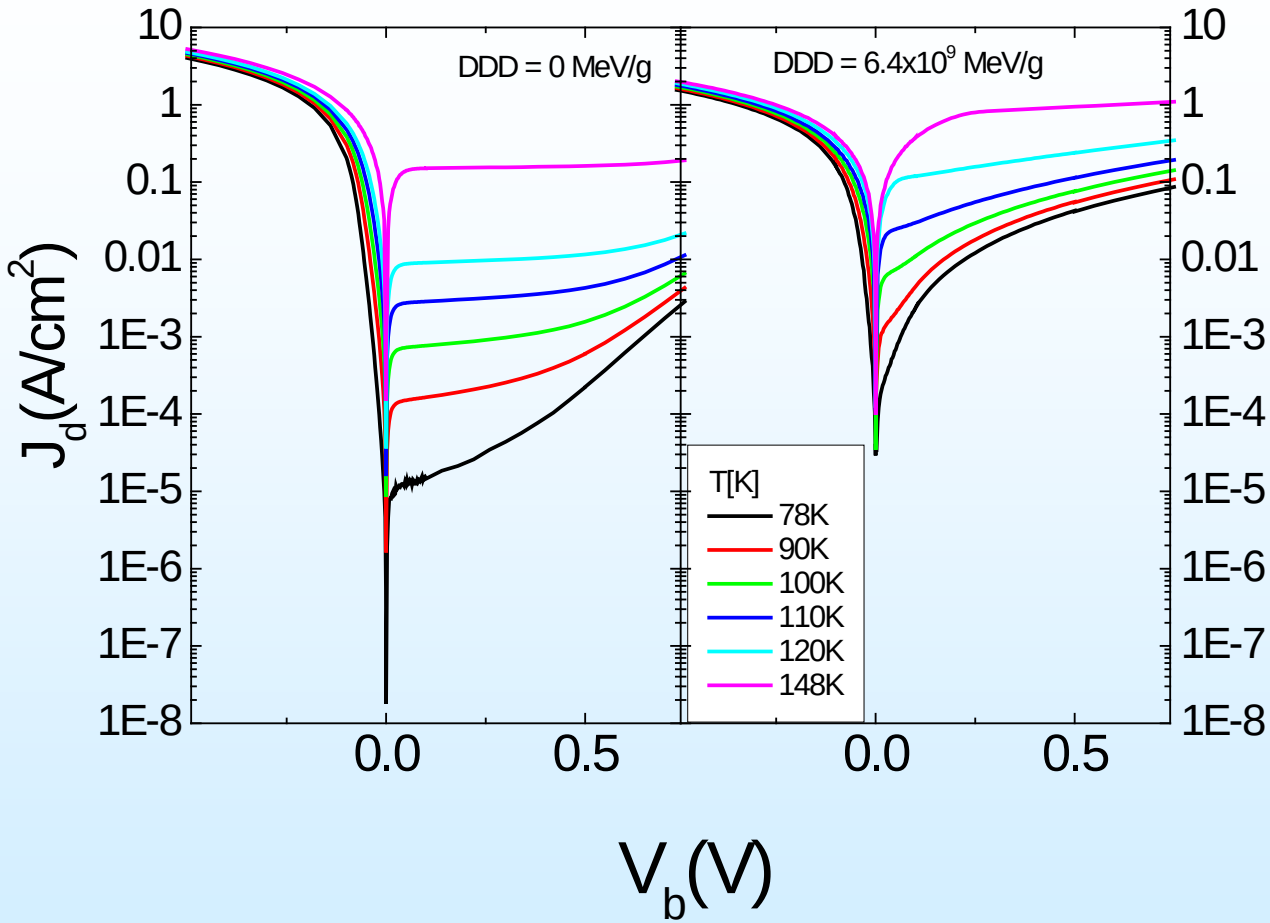

The dark current density vs. applied bias at different operating temperatures

Left: before irradiation (DDD = 0)

Right: after the last irradiation, DDD = 6.4×10^9 MeV/g

Copyright 2011. All rights reserved.

Arrhenius analysis

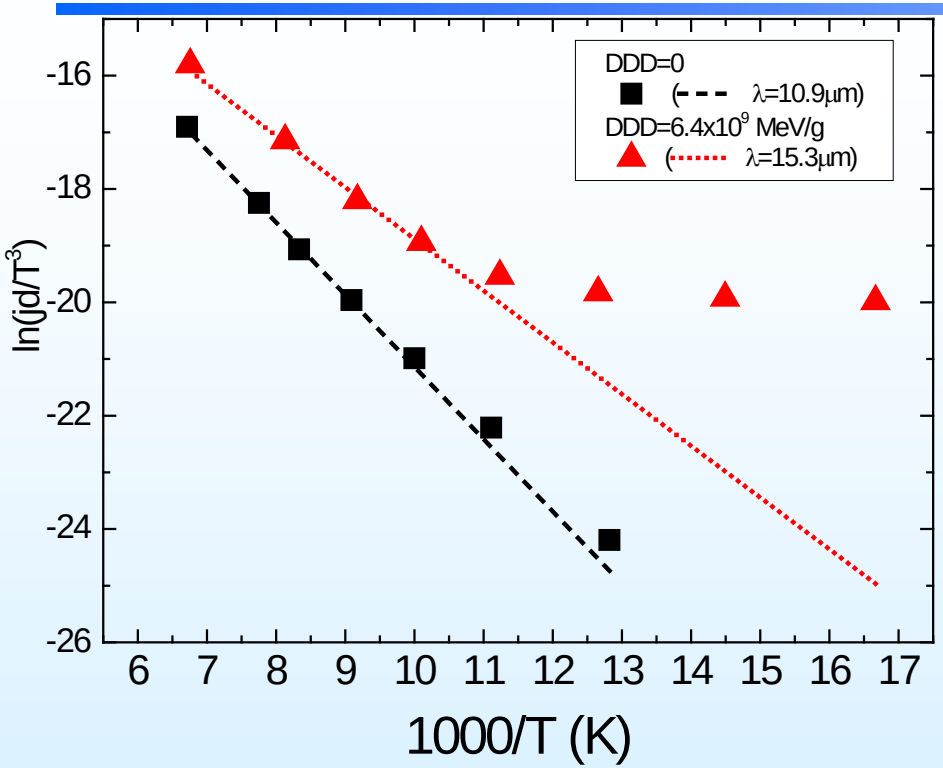

Expression for the diffusion dark current $j_{diff} \sim T^3 \exp(-Eg/k_B T)$ is used for evaluation of the temperature dependence

- **Before radiation (DDD = 0)**
  - The activation energy is E_{fg} = 0.115 meV
  - Close to the superlattice bandgap value, Eg = 0.12 meV
  - Diffusion dark current
- **After irradiation (DDD = 6.4 × 10^9 MeV/g)**
  - The dark current becomes temperature independent at around T = 95K
    - Tunneling current becomes the dominant source of the dark current at lower temperature
  - Moreover, the $E_{fg} \approx$ 0.080 meV in the range T = 100 - 150 K
    - This is about 75% of the superlattice bandgap.
    - Indicates combination of the diffusion and generation-recombination processes.

Copyright 2011. All rights reserved.

Dark current mechanisms

Further understanding of the dark current mechanism changes with irradiation can be inferred from studies of the dark current dependence on the applied bias.

The three major sources of dark current in the InAs/GaSb photodioides are:

- Diffusion (j_{diff})
- Generation-recombination ($j_{g\text{-}r}$)
- Tunneling (j_{tunn})
  - -At low biases mostly due to trap assisted tunneling

- The diffusion dark current: $\boldsymbol{j_{diff} = J_0\, exp(qV/k_BT)\text{-}1)}$

  J_0 is saturation current, V is applied bias, q is electron charge, and k_B is Boltzmann constant

- Generation-recombination current : $\boldsymbol{j_{g-r} = A_{g-r}\, \frac{1}{V_{bi}-V} \sinh\left(-\frac{qV}{2k_BT}\right) \frac{\ln(\sqrt{b^2-1}+b)}{\sqrt{b^2-1}}}$;

  $b = e^{-\frac{qV}{2k_BT}}$, where $A_{g\text{-}r}$ is a constant and V_{bi} is built in potential.

- Trap assisted tunneling current: $\boldsymbol{j_{tunn} = A_{TAT} V exp\left(-\frac{B}{\sqrt{V_{bi}-V}}\right)}$

  A_{TAT} and B_{TAT} are voltage independent constants.

Copyright 2011. All rights reserved.

J_d vs V fit

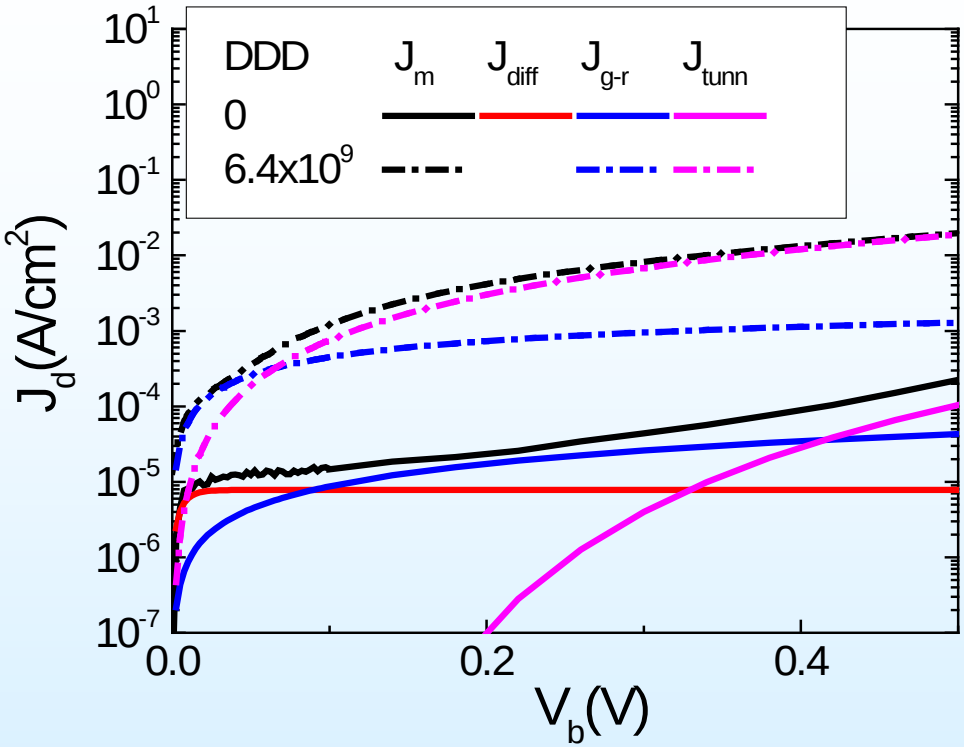

Fit of measured dark current density, j_m, at T = 80 K for DDD = 0 and 6.4 ×10^9 MeV/g with diffusion (j_{diff}), generation-recombination (j_{g-r}) and tunneling (j_{tunn}) components.

- Before irradiation:
  - Diffusion dark current for V_b <100mV.
  - Generation-recombination current starts to dominate at higher bias
  - Tunneling current becomes the prevailing component at the applied biases above 400 mV
- After irradiation with DDD = 6.4×10^9 MeV/g:
  - Generation-recombination current dominates at Vb < 50 mV and
  - Tunneling current starts to dominate at higher bias
- These results are in good agreement with the conclusions from the J_d temperature dependence

Surface leakage current

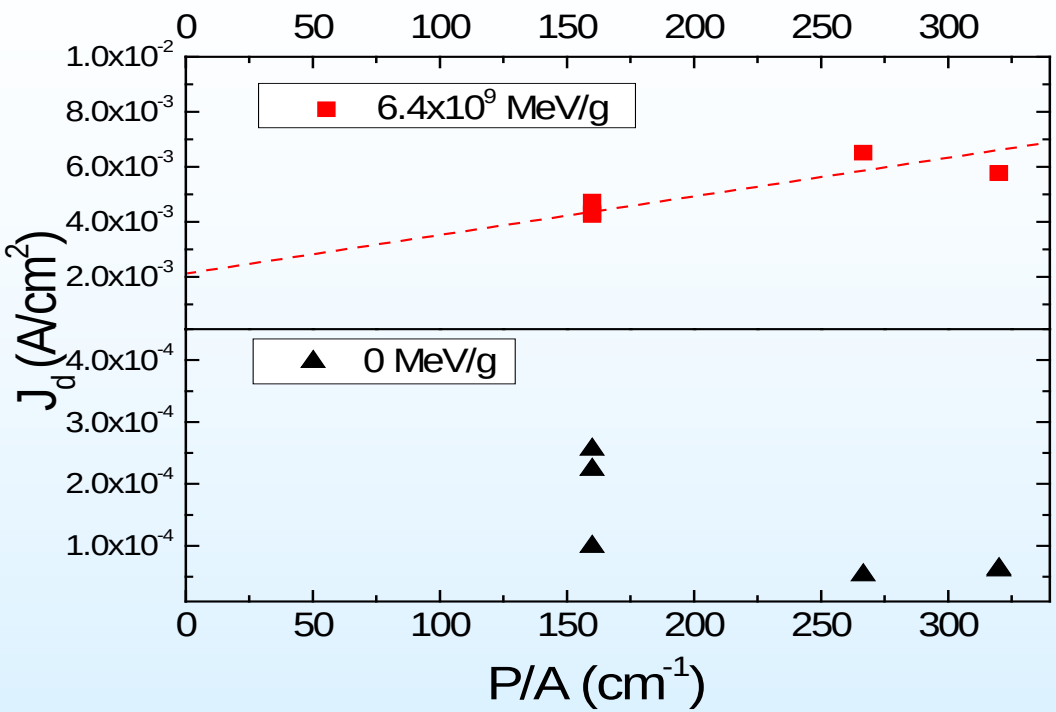

The dark current density:

$j_d = j_b + j_s \times P/A$

j_b is bulk current densities

j_s is surface current densities

- Before the irradiation: No clear dark current dependence on the perimeter/area, P/A, ratio
- After irradiation: Linear dependence of the dark current on the perimeter/area is observed

  Fitted bulk current: $j_{ba} \approx 2\times10^{-3}$ A/cm^2
- Irradiation increases both bulk and surface dark currents

  Damage near the detector side wall has a larger effect on the dark current
- Surface dark currents observed here arises from the tunneling through defects created by the radiation near the device side walls

Copyright 2011. All rights reserved.

QE change with radiation

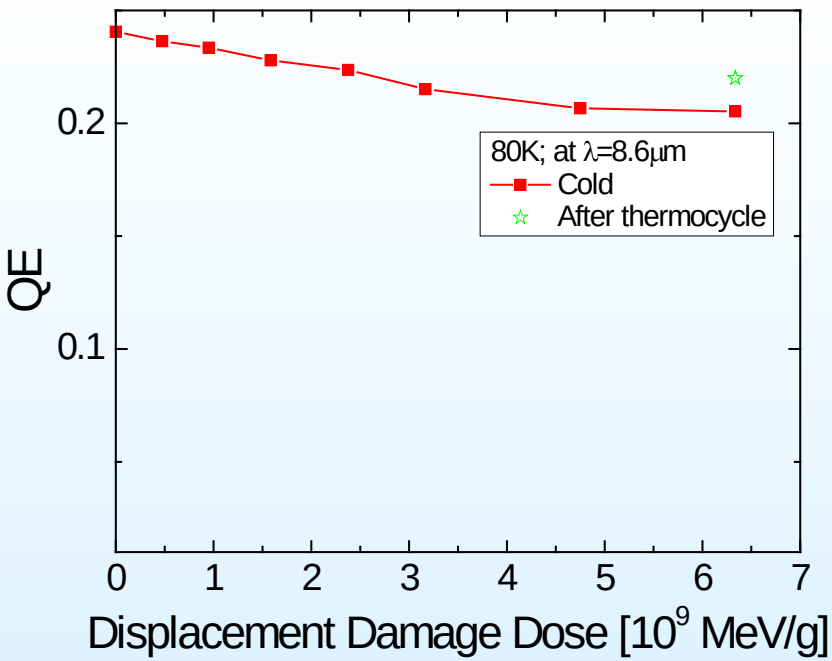

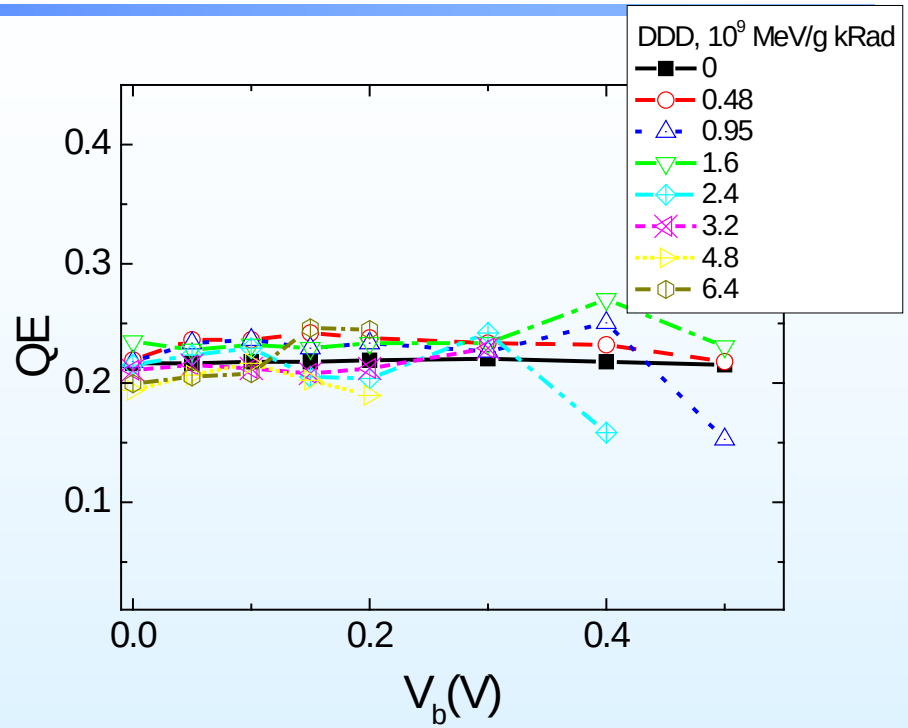

- Before irradiation: $QE_B \approx 0.24$ at $\lambda = 8.6\mu m$
- QE_B decreases with radiation dose

  $QE_B \approx 0.21$ at DDD = 6.4×10^9 MeV/g.

  15% decrease in QE over the full range of DDD.
- Detector thermocycling: minor increase of QE to $QE_B \approx 0.22$
- No change in turn-on bias, V_{on}

Copyright 2011. All rights reserved.

Why only small change in QE

Two hypothesis

1. $L_e >> d$:

- From transmission measurements:
  - Measured absorption coefficient (α): $\alpha \sim 2500$ cm^{-1} at $\lambda = 7$ μm
  - Substrate transmission is found to be close to 100% at this wavelength
- Estimate the minority carriers (electrons) diffusion length, L_e, from the absorption coefficient and QE value.
  - $L_e \approx$ 5-6 μm is significantly longer than the absorber thickness $d = 2$ μm.
- In this regime, $L_e >> d$, the decrease of the diffusion length with DDD would only result in a small degradation of QE.

2. Only a minor decrease of the lifetime with radiation?

- Minority carrier lifetime in LWIR InAs/GaSb superlattice is relatively short, $\tau \approx 30$ ns
  - Due to the non-radiative recombination through defects states associated with Ga atoms and potentially assisted by multiphonon processes.
- The defects are intrinsically present in the superlattice and can continue to dominate the recombination process even after exposure to the radiation

Copyright 2011. All rights reserved.

Summary

- The antimonide material system provides
  - Added material robustness for manufacturability
  - Variety of band offsets for flexibility in design
  - Large-area substrates for large format arrays/economy of scale
- Complementary Barrier Infrared Detector (CBIRD)
- High-performance superlattice FPAs based on n-CBIRD

  - Operability ~ 97% [$0.75*R_{MEAN} < R < 1.25*R_{MEAN}$]

  - QE ~ 45% (4.5 – 9 µm)

  - NEDT ~ 18.6 mK
- Single pixel devices on PEC vs FPA
  - Room for improvement
  - Need better understanding of dark current mechanisms
- Proton irradiation effects
  - Increase in dark current due to onset of surface leakage current
  - Small decrease in quantum efficency